



**Deterministic generation of phononic Fock states via weak nonlinearities**Yi-Xuan Ma  and Peng-Bo Li \**Ministry of Education Key Laboratory for Nonequilibrium Synthesis and Modulation of Condensed Matter, Shaanxi Province Key Laboratory of Quantum Information and Quantum Optoelectronic Devices, School of Physics, Xi'an Jiaotong University, Xi'an 710049, China*

(Received 6 June 2023; accepted 19 October 2023; published 13 November 2023)

We propose an efficient method to generate single-phonon Fock states by exploiting a previously unidentified phonon blockade mechanism in a hybrid spin-mechanical system. Specifically, this mechanism makes use of arbitrarily weak Duffing nonlinearity to modify matrix elements of an effective phonon excitation process, assisted by both one- and two-phonon drives. The weak Duffing nonlinearity of the phonons is induced by a nitrogen-vacancy (NV) center magnetically coupled to a cantilever, while the mechanical parametric driving is realized by modulating the spring constant of the cantilever using a pump. By implementing a time-dependent protocol for the linear and parametric drives, there exists a strict cutoff in the phonon number distribution, resulting in a pure Fock state. Furthermore, the nonclassical nature of the generated state remains robust against dissipations.

DOI: [10.1103/PhysRevA.108.053709](https://doi.org/10.1103/PhysRevA.108.053709)**I. INTRODUCTION**

Quantum behaviors of nanomechanical resonators have received much interest recently. The hybrid spin-mechanical system, which combines the long coherence time of solid-state spins and the high-quality factors of nanomechanical resonators [1–9], has been widely applied in different fields such as quantum information science [7,10–24] and quantum sensing [18].

Rich quantum mechanical effects can be explored in hybrid spin-mechanical systems, such as phonon blockade (PB) [25–34], which can be exploited to prepare Fock states. It is akin to photon blockade in cavity QED [35–45], and it refers to the phenomenon that the presence of a single phonon prevents the excitation of subsequent phonons. Thus, it is a promising mechanism as a single-phonon source [46]. Nonlinearity is typically of essential importance to realize this nonclassical effect. It is either intrinsic or induced through coupling to an auxiliary system such as a qubit [25,26,46–48]. Conventional phonon blockade (CPNB) is achieved due to the anharmonicity of the eigenstates in the presence of strong nonlinearity [25,26,49–54]. CPNB is difficult to realize when nanomechanical resonators have only intrinsic nonlinearities, which are typically weak [34,55]. However, by exploiting the destructive interference between different paths, the excitation of two phonons is blocked in arbitrarily weak nonlinear systems [56,57], which is known as unconventional phonon blockade (UCPNB). Unfortunately, the parameter window for destructive interference is very narrow, and a tiny deviation from the ideal condition will seriously destroy the UCPNB phenomenon. Furthermore, both CPNB and UCPNB lack a true cutoff for higher excitations [58].

In this work, we adopt another mechanism to generate a single-phonon Fock state in a spin-mechanical system, where a nanomechanical resonator is magnetically coupled to a single nitrogen-vacancy (NV) center. In such a hybrid system, the NV spin dispersively interacts with the mechanical resonator to induce weak Duffing nonlinearities for the phonons. An electric pump modulating the spring constant of the mechanical cantilever is applied to realize the parametric drives [23], which can be easily implemented in experiments. Through a time-dependent protocol modulating the linear and parametric drives, the matrix element for transitions from the one-phonon to the two-phonon state equals zero, even with arbitrarily weak phononic nonlinearity. Therefore, a truly blocked state can be generated and the average phonon number of the specific intermediate state is exactly 1. We visualize topographies of our operation to show the true blockade physics and how transitions to other states are activated when the parameters are not tuned perfectly. We also show that the nonclassical properties of the generated state are robust against dissipation due to the strong negativity of the Wigner function.

This paper is organized as follows. In Sec. II, we describe the hybrid spin-mechanical system that we focus on, showing how the Duffing nonlinearity for phonon blockade is induced. In Sec. III, we discuss the time-dependent protocol for the generation of Fock states based on phonon blockade and how the physics is challenged with parameter mismatching and dissipations. The robust nonclassicality is also presented via the visualization of the Wigner function. In Sec. IV, we discuss how to detect the Fock state in our system. In Sec. V, we show that the method is feasible in current experimental platforms. We conclude in Sec. VI.

**II. SETUP**

Our discussion is focused on a specific system as shown in Fig. 1, where a nanomechanical resonator interacts with a

\*lipengbo@mail.xjtu.edu.cn

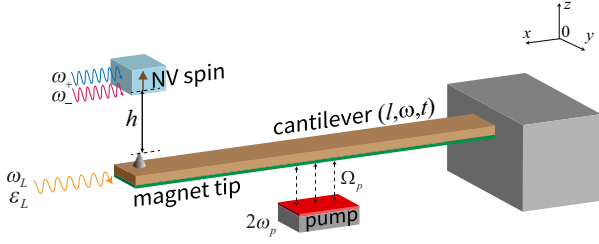


FIG. 1. Illustration of the spin-mechanical coupling system of our interest. The spin of the NV center is magnetically coupled to the vibration mode of the cantilever. One electrode is attached to the lower surface of the cantilever beam and the other is placed under the cantilever beam to form a capacitor. The electric field from the capacitor modifies the spring constant of the cantilever. A strong linear drive is also applied.

single NV center [59]. We set a magnet tip at the end of the cantilever and place the NV center near it. As the cantilever vibrates, the magnet tip produces a time-dependent magnetic field at the position of the NV center so that spin-phonon coupling is induced. We perform a periodic electrical pump to modulate the cantilever's spring constant with amplitude  $\Omega_p$  and frequency  $\omega_p$ , which can generate the mechanical parametric drive [23]. A classic-field linear mechanical drive is also applied with amplitude  $\varepsilon_L$  and frequency  $\omega_L$ .

The Hamiltonian of the cantilever is given by [23]

$$\hat{H}_{\text{mec}} = \omega_m \hat{a}^\dagger \hat{a} + \Omega_p \cos(2\omega_p t) (\hat{a}^\dagger + \hat{a})^2 + \varepsilon_L (\hat{a}^\dagger e^{-i\omega_L t} + \hat{a} e^{i\omega_L t}), \quad (1)$$

where  $\hat{a}$  and  $\hat{a}^\dagger$  are the annihilation and creation operators of the oscillating mode  $\omega_m$ . As shown in Fig. 2(a), the zero field splitting between  $|m_s = \pm 1\rangle$  and the ground state  $|m_s = 0\rangle$  is  $D = 2\pi \times 2.87$  GHz. An external static magnetic field induces the Zeeman splitting  $\delta_z = 2g_e \mu_B B_s$ , where  $g_e \simeq 2$  and  $\mu_B = 14$  GHz/T. The two microwave magnetic fields in the  $x$  direction  $B_x^\pm(t) = B_0^\pm \cos \omega_\pm t$  help to adjust the energy level, with Rabi frequencies  $\Omega_\pm = g_e \mu_B B_0^\pm$  and detunings  $\Delta_\pm = D \pm \delta_z/2 - \omega_\pm$ . For simplicity, we require  $\Omega_\pm = \Omega$  and  $\Delta_\pm = \Delta$ . In the rotating frame with respect to the two microwave frequencies, the Hamiltonian for the NV center is

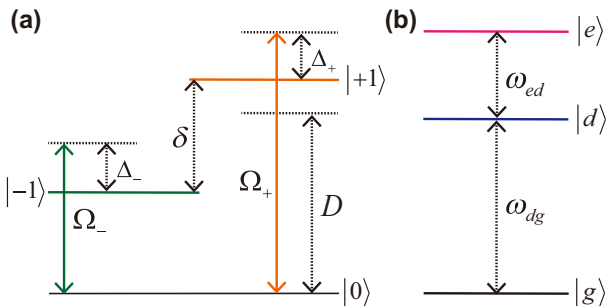


FIG. 2. The energy level of the NV center. (a) The energies for the spin-triplet.  $|1\rangle$ ,  $|-1\rangle$  are split by a magnetic field. (b) The energy level of the dressed states. The energy difference between  $|e\rangle$  and  $|d\rangle$  is significantly smaller than that between  $|d\rangle$  and  $|g\rangle$ .

given by [59]

$$\hat{H}_{\text{NV}} = \sum_{j=\pm} \Delta |j\rangle \langle j| + \frac{\Omega}{2} (|j\rangle \langle 0| + |0\rangle \langle j|). \quad (2)$$

Now we turn to spin-phonon interaction. The interaction Hamiltonian  $\hat{H}_{\text{int}} = \mu_B g_e \hat{\mathbf{S}} \cdot \mathbf{B}(\mathbf{r}_0)$ , where  $\mathbf{r}_0$  is the position of the NV center and  $\hat{\mathbf{S}}$  is the spin operator. We assume the resonator only vibrates in the  $z$  direction. Thus we can expand the Hamiltonian as  $\hat{H}_{\text{int}} \simeq \frac{1}{2} \mu_B g_e G \hat{z} \hat{\mathcal{S}}_z$ , where  $G = \partial B_z / \partial z(\mathbf{r}_0)$ . Using the phonon's annihilation and creation operators which give  $\hat{z} = z_{\text{zpf}}(\hat{a}^\dagger + \hat{a})$ , we have

$$\hat{H}_{\text{int}} \simeq g(\hat{a}^\dagger + \hat{a}) \hat{\mathcal{S}}_z. \quad (3)$$

Thus, we obtain the total Hamiltonian

$$\hat{H}_{\text{Total}} = \hat{H}_{\text{mec}} + \hat{H}_{\text{NV}} + \hat{H}_{\text{int}}. \quad (4)$$

We next switch to the dressed states. Note that  $\hat{H}_{\text{NV}}$  induces the state transformation from  $|0\rangle$  to the bright state  $|b\rangle = (|+1\rangle + |-1\rangle)/\sqrt{2}$ , but leaves the dark state  $|d\rangle = (|+1\rangle - |-1\rangle)/\sqrt{2}$  decoupled. Therefore, the eigenstates of  $\hat{H}_{\text{NV}}$  consist of  $|d\rangle$  and two other dressed states  $|g\rangle = \cos \theta |0\rangle - \sin \theta |b\rangle$  and  $|e\rangle = \sin \theta |0\rangle + \cos \theta |b\rangle$ , where  $\tan(2\theta) = -\sqrt{2}\Omega/\Delta$ . We consider the case of large detuning, where both the spin-mechanical coupling and the microwave magnetic field are weak. This requires that  $\omega_m - \omega_{ed} \gg g$  and  $\Delta \gg \Omega$  [60]. Therefore, we have  $\omega_{dg} \gg \omega_{ed} \simeq \Omega^2/2\Delta$ , so that  $|g\rangle$  can be ignored and the NV center can be treated as a two-level system (TLS). The Hamiltonian is simplified to

$$\begin{aligned} \hat{H}_{\text{Total}} \simeq & \omega_m \hat{a}^\dagger \hat{a} + \omega_{ed} \hat{\sigma}_+ \hat{\sigma}_- + g(\hat{a}^\dagger + \hat{a})(\hat{\sigma}_+ + \hat{\sigma}_-) \\ & + \Omega_p \cos(2\omega_p t) (\hat{a}^\dagger + \hat{a})^2 \\ & + \varepsilon_L (\hat{a}^\dagger e^{-i\omega_L t} + \hat{a} e^{i\omega_L t}), \end{aligned} \quad (5)$$

where  $\hat{\sigma}_+ = |e\rangle \langle d|$ . We perform a unitary transformation  $\hat{U} = e^{-i\hat{H}_0 t}$ , where  $\hat{H}_0 = \omega_p (\hat{a}^\dagger \hat{a} + |e\rangle \langle e|)$ , requiring  $\omega_p \gg \{\Omega_p, g\}$  and  $\omega_L = \omega_p$ . In this case, we have

$$\begin{aligned} \hat{H}_{\text{Total}} \simeq & \hat{H}_{\text{JC}} + \hat{H}_{\text{drive}} \\ = & \delta_m \hat{a}^\dagger \hat{a} + \delta_{ed} \hat{\sigma}_+ \hat{\sigma}_- + g(\hat{a}^\dagger \hat{\sigma}_- + \hat{a} \hat{\sigma}_+) \\ & + \frac{\Omega_p}{2} (\hat{a}^{\dagger 2} + \hat{a}^2) + \varepsilon_L (\hat{a}^\dagger + \hat{a}), \end{aligned} \quad (6)$$

where  $\delta_{m(ed)} = \omega_{m(ed)} - \omega_p$ .

We then follow the method discussed in [61] to get the effective Hamiltonian with high accuracy. According to the large-detuning condition,  $\lambda = g/|\omega_{ed} - \omega_m| = g/|\Delta|$  is a small quantity. With the unitary transformation  $\hat{D} = \exp[-\Lambda(\hat{N}_q)(\hat{a}^\dagger \hat{\sigma}_- - \hat{a} \hat{\sigma}_+)]$ , where

$$\Lambda(\hat{N}_q) = -\frac{\arctan(2\lambda\sqrt{\hat{N}_q})}{2\sqrt{\hat{N}_q}}, \quad (7)$$

and  $\hat{N}_q$  is the total excitation number

$$\hat{N}_q = \hat{a}^\dagger \hat{a} + |e\rangle \langle e|, \quad (8)$$

we can accurately diagonalize the Jaynes-Cummings (JC) model part of Eq. (6) as follows:

$$\hat{H}_{\text{JC}}^D = \delta_m \hat{a}^\dagger \hat{a} + \delta_{ed} \hat{\sigma}_+ \hat{\sigma}_- - \frac{\hbar \Delta'}{2} (1 - \sqrt{1 + 4\lambda^2 \hat{N}_q}) \hat{\sigma}_z. \quad (9)$$

Since the qubit is dressed by the field in our new basis, the transformed field operator contains the qubit part as well

$$\hat{a}^D \approx \hat{a} \left( 1 + \frac{\lambda^2 \hat{\sigma}_z}{2} \right) + \lambda \left[ 1 - 3\lambda^2 \left( \hat{a}^\dagger \hat{a} + \frac{1}{2} \right) \right] \hat{\sigma}_- + \lambda^3 \hat{a}^2 \hat{\sigma}_+. \quad (10)$$

We assume that the TLS is prepared in the excited state  $|e\rangle$  initially. Under the weak interaction with the mechanical system, it is reasonable to assume the state of the TLS is frozen, so we can diminish the dependence of the TLS in Eq. (6). Finally, we obtain the effective Hamiltonian of the mechanical system

$$\hat{H}_{\text{eff}} = U \hat{a}^\dagger \hat{a}^\dagger \hat{a} \hat{a} + \delta \hat{a}^\dagger \hat{a} + (\varepsilon_1 \hat{a}^\dagger + \varepsilon_2 \hat{a}^\dagger \hat{a}^\dagger + \text{H.c.}), \quad (11)$$

where the first term corresponds to the Duffing nonlinearity with amplitude  $U = -g\lambda^3$ , the second term is the free Hamiltonian with detuning  $\delta = \delta_m + g\lambda$ , and the last two terms describe the one- and two-phonon driving with amplitudes  $\varepsilon_1 = \varepsilon_L (1 + \frac{1}{2}\lambda^2)$  and  $\varepsilon_2 = \frac{\Omega_p}{2} (1 + \lambda^2)$ , respectively.

### III. GENERATION OF FOCK STATE

Now we realized the linear and parametric drives, as well as the Duffing nonlinearity in a spin-mechanical system as displayed in Eq. (11). We will present in the following that these ingredients are sufficient for phonon blockade and single-phonon generation even if the Duffing nonlinearity is arbitrarily weak [45].

Note that the Duffing nonlinearity term in Eq. (11) is relatively weak. However, the effect of this nonlinearity can be enhanced by quick linear driving, i.e., a displacement in phase space. From the view of passive transformation, it equals to a change of  $\hat{a} \rightarrow \hat{a} + \alpha$ , where  $|\alpha|$  is a large quantity. The Hamiltonian is transformed to

$$\hat{H}_\alpha = U \hat{a}^\dagger \hat{a}^\dagger \hat{a} \hat{a} + \tilde{\delta} \hat{a}^\dagger \hat{a} + (\tilde{\varepsilon}_1 \hat{a}^\dagger + \tilde{\varepsilon}_2 \hat{a}^\dagger \hat{a}^\dagger + \Lambda \hat{a}^\dagger \hat{a}^\dagger \hat{a} + \text{H.c.}), \quad (12)$$

where the parameters are changed into

$$\tilde{\delta} = \delta + 4U|\alpha|^2, \quad (13a)$$

$$\tilde{\varepsilon}_1 = \varepsilon_1 + \alpha\delta + 2\alpha^* \varepsilon_2 + 2U|\alpha|^2 \alpha, \quad (13b)$$

$$\tilde{\varepsilon}_2 = \varepsilon_2 + U\alpha^2, \quad (13c)$$

$$\Lambda = 2U\alpha. \quad (13d)$$

By requiring parameters tuned as

$$\varepsilon_1 = \Lambda(-r + |\Lambda|^2/2U^2), \quad (14a)$$

$$\varepsilon_2 = -\Lambda^2/4U, \quad (14b)$$

$$\delta = -|\Lambda|^2/U, \quad (14c)$$

we have  $\hat{H}_{\text{target}}$  in the displaced frame

$$\hat{H}_{\text{target}} = [\Lambda \hat{a}^\dagger (\hat{a}^\dagger \hat{a} - r) + \text{H.c.}] + U \hat{a}^\dagger \hat{a}^\dagger \hat{a} \hat{a}. \quad (15)$$

An exotic nonlinear term  $\hat{a}^\dagger \hat{a}^\dagger \hat{a}$  emerges, with its strength  $\Lambda$  significantly greater than the weak Duffing nonlinearity  $U$ . Taking  $r = 1$ , it is obvious that the transition from  $|1\rangle$  to  $|2\rangle$  is forbidden. To be specific, starting with the vacuum of the displaced frame, the system will go through Rabi oscillation in the blockaded subspace  $\{|0\rangle, |1\rangle\}$ . Then let the

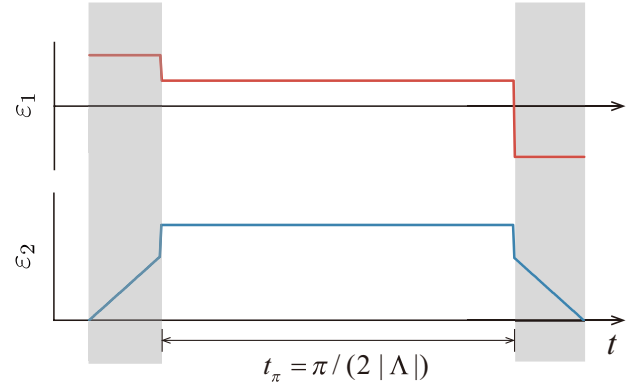


FIG. 3. Time-dependent protocol for linear and parametric drives. We use  $\varepsilon_1$  to drive the vacuum to the coherent state  $|\alpha\rangle$  initially and drive the displaced-frame Fock state back to the laboratory frame in the end. One and two phonon drives are tuned as Eqs. (14a) and (14c) in the displaced frame and the evolution time is controlled to  $t_\pi$ .

system evolve for  $t_\pi = \pi/(2|\Lambda|)$ , we can obtain the accurate displaced-frame Fock state.

Finally, applying the linear driving again with its phase changing  $\pi$ , the Fock state in the laboratory frame is obtained. The time-dependent protocol of  $\varepsilon_1$  and  $\varepsilon_2$  is illustrated in Fig. 3. In the initial and final displacements, parametric drives are also applied to correct the squeezing by the Duffing nonlinearity.

#### A. Impact of deviations from perfect drive-amplitude matching

Perfect parameter matching according to Eq. (14) is unreachable in experiments. Deviation of  $\varepsilon_1$  equals to a change of  $r = 1 + \delta r_1$ . Deviation of  $\varepsilon_2$  will introduce a redundant mechanical parametric amplification (MPA) term  $\Lambda \delta r_2 \hat{a}^\dagger \hat{a}^\dagger$  in Eq. (15), which induces the transition from  $|0\rangle$  to  $|2\rangle$ . We will show even in the presence of parameter mismatching, the generated state remains a good approximation of the Fock state.

We focus on the intermediate physics for Fock state generation. In Fig. 4 we present the tomographies of the time evolution operator  $\hat{U} = \exp(-i\hat{H}t_\pi)$  and the output state to visualize the operation made to the system. We check the impact of small  $\delta r_1$  and  $\delta r_2$ , respectively, in Figs. 4(b) and 4(c). For imperfectly tuned  $\varepsilon_1$ , there is a weak leakage from  $|1\rangle$  to  $|2\rangle$ . Nonzero  $\delta r_2$  activates the transition between  $|0\rangle$  and  $|2\rangle$ . Nonetheless,  $|1\rangle$  is still the dominant component for the two situations.

Next, we investigate the deviation of phonon blockade when there are deviations of both  $\varepsilon_1$  and  $\varepsilon_2$ . Let us consider the short time after the beginning of the evolution, with almost no leakage to  $|3\rangle$ . The instantaneous  $g^{(2)}(0; t)$  is given by

$$g^{(2)}(0; t) = \delta r_1^2 + \frac{4\delta r_2^2}{|\Lambda|^2 t^2}. \quad (16)$$

The existence of  $\delta r_2$  results in a divergence at  $t = 0$  since  $|1\rangle$  and  $|2\rangle$  are both able to be transferred from  $|0\rangle$  directly at the very beginning. However, the total  $g^{(2)}(0; t)$  decreases rapidly with time as the population on  $|1\rangle$  increases.

The time-dependent probabilities for  $|n\rangle$  (denoted by  $P_n$ ) are shown in Fig. 5(a). Compared with the pure state  $|1\rangle$ , the fidelity  $F$  equals approximately to  $P_1$  [62]. It is always 1

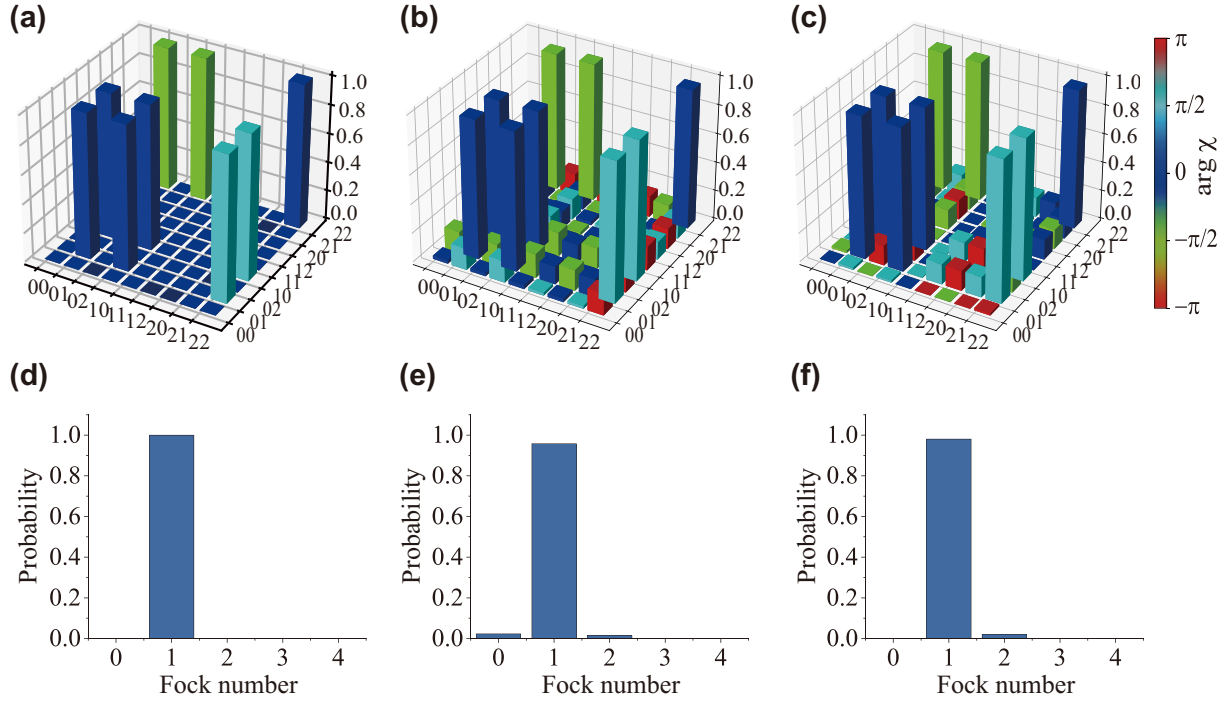


FIG. 4. The effect of parameter mismatching. Quantum process tomographies of the operation (where “ $i$ ” denotes the operator  $|i\rangle\langle j|$ ) and Fock distributions of the output state are plotted, with each column corresponding to the same parameters. (a), (d) Perfect parameter matching with  $\delta r_1 = 0$  and  $\delta r_2 = 0$ . If the initial state is tuned to  $|0\rangle$ , such an operation will output the ideal  $|1\rangle$ . Imperfect parameter matching with (b), (e)  $\delta r_1 = 0.1$  and (c), (f)  $\delta r_2 = 0.1$ , respectively. Transition to  $|2\rangle$  is activated, but the population on  $|1\rangle$  is still approximately 1.

with perfectly matched parameters. In contrast, with  $\delta r_1 = 0.1$  and  $\delta r_2 = 0.1$ , the fidelity decreases to 0.94. We compare the effect of these two parameter mismatchings in Figs. 5(c) and 5(d). The average phonon number is very close to 1 even with  $\delta r_1 = 0.2$  and  $\delta r_2 = 0.2$ .

### B. Phonon blockade in dissipative systems

So far, we assumed an ideal closed system. For open quantum systems with dissipation, the time evolution of the

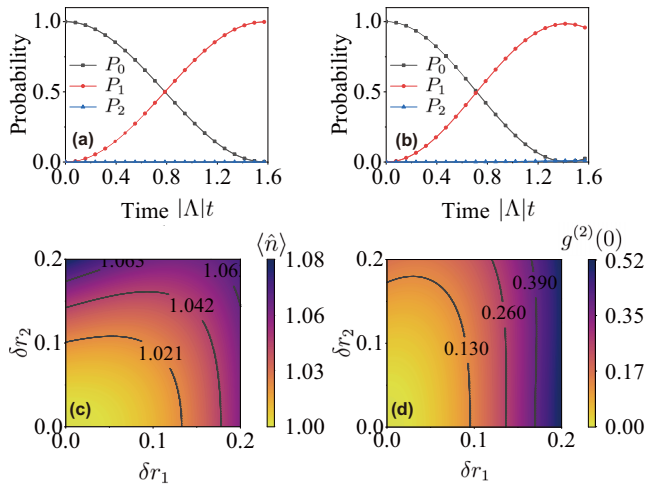


FIG. 5. Time evolution of  $n$ -phonon probabilities and fidelity with (a) perfectly tuned parameters (b)  $\delta r_1 = 0.1$  and  $\delta r_2 = 0.1$ . (c) Average phonon number  $\langle \hat{n} \rangle$  and (d) correlation function  $g^{(2)}(0)$  versus one- and two-phonon drive amplitude mismatching.

reduced density matrix under Markovian approximation can be described by the Lindblad master equation

$$\begin{aligned} \dot{\hat{\rho}} = & -i[\hat{H}_{\text{eff}}, \hat{\rho}] + \frac{\gamma}{2}n_{\text{th}}(2\hat{a}^\dagger\hat{\rho}\hat{a} - \hat{a}\hat{a}^\dagger\hat{\rho} - \hat{\rho}\hat{a}\hat{a}^\dagger) \\ & + \frac{\gamma}{2}(n_{\text{th}} + 1)(2\hat{a}\hat{\rho}\hat{a}^\dagger - \hat{a}^\dagger\hat{a}\hat{\rho} - \hat{\rho}\hat{a}^\dagger\hat{a}), \end{aligned} \quad (17)$$

where  $\gamma$  is the damping constant for the resonator.  $n_{\text{th}}$  is the average phonon number related to environmental temperature ( $n_{\text{th}} = 1/\{\exp[\hbar\omega/(k_B T)] - 1\}$ ).

Note that Eq. (17) is written in the laboratory frame. Displacing the dissipator changes  $\hat{a}$  to  $\hat{a} + \alpha$ , inducing a coherent linear drive [45]

$$\begin{aligned} \dot{\hat{\rho}} = & -i\left[\hat{H}_{\text{target}} - \left(\frac{1}{2}i\alpha\gamma a^\dagger + \text{H.c.}\right), \hat{\rho}\right] \\ & + \frac{\gamma}{2}n_{\text{th}}(2\hat{a}^\dagger\hat{\rho}\hat{a} - \hat{a}\hat{a}^\dagger\hat{\rho} - \hat{\rho}\hat{a}\hat{a}^\dagger) \\ & + \frac{\gamma}{2}(n_{\text{th}} + 1)(2\hat{a}\hat{\rho}\hat{a}^\dagger - \hat{a}^\dagger\hat{a}\hat{\rho} - \hat{\rho}\hat{a}^\dagger\hat{a}), \end{aligned} \quad (18)$$

which can be absorbed into  $\tilde{\epsilon}_1$ :

$$\tilde{\epsilon}_1 = \epsilon_1 + \alpha\delta + 2\alpha^*\epsilon_2 + 2U|\alpha|^2\alpha - \frac{1}{2}i\gamma\alpha. \quad (19)$$

To compensate for the induced linear drive,  $\epsilon_1$  needs to be tuned as

$$\epsilon_1 = \Lambda \left( -r + \frac{|\Lambda|^2}{2U^2} + \frac{i\gamma}{4U} \right) \quad (20)$$

so that Eq. (14a) is modified.

We plot the evolution of probability distributions  $P_n$  in Fig. 6(a). To demonstrate the effects of the environment on



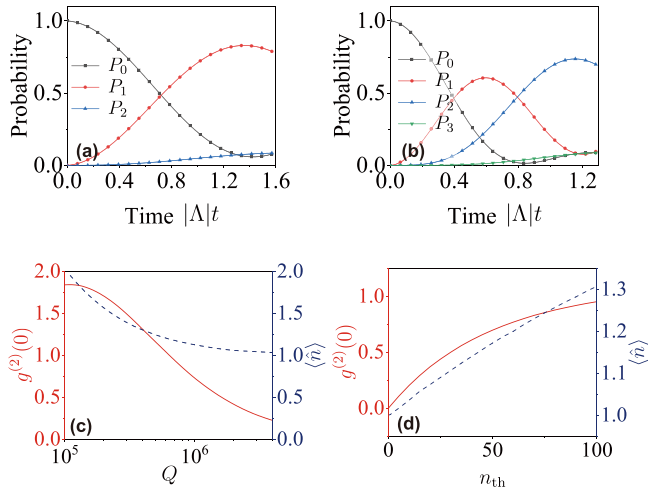


FIG. 6. Time evolution of  $n$ -phonon probabilities and fidelity with dissipation for (a)  $r = 1$  and (b)  $r = 2$ . The mismatches are still set as  $\delta r_1 = 0.1$  and  $\delta r_2 = 0.1$ . Average phonon number and correlation function versus (c)  $Q$  factor and (d) thermal phonon number. The damping constant  $\gamma$  is set to  $0.0033\Lambda$  except for (c) and average thermal phonon  $n_{\text{th}}$  is set to 20 except for (d), as discussed in Sec. V.

the nanomechanical resonator, we plot the change of  $\langle \hat{n} \rangle$  and  $g^{(2)}(0)$  versus  $Q$  and  $n_{\text{th}}$  in Figs. 6(c) and 6(d). Unsurprisingly, the blockade physics is stronger with higher  $Q$  and lower  $n_{\text{th}}$ . We point out that  $\Lambda \sim \alpha$ , while  $\varepsilon_1 \sim \alpha^3$  and  $\varepsilon_2 \sim \alpha^2$ . Since  $\alpha$  is a large quantity (in Sec. V our evaluation gives  $|\alpha| > 10^2$ ),  $\Lambda$  is much smaller than  $\varepsilon_1$  and  $\varepsilon_2$ . According to the master equation, moving to the displaced frame makes the system more fragile to decoherence. However, when the quality factor is  $10^6$  and the thermal phonon number is 20, which is reachable in experiments, we can still obtain the desirable Fock state, with the average phonon number  $\langle \hat{n} \rangle$  very close to 1. The fidelity equals 0.79 in this case.

Our method is not limited to generating  $|1\rangle$ . More generally, by setting  $r$  to any integer  $n$ , the transition matrix element from  $|n\rangle$  to  $|n+1\rangle$  is zero. Thus, the mechanism is also valid for the  $n$ -phonon blockade as well as generating  $|n\rangle$ . Note that the evolution time differs for different  $n$ . For  $n = 2$ , the system should evolve for  $t_2 \approx \pi/\sqrt{6}|\Lambda|$  to maximize the average phonon number as shown in Fig. 6(b). However, the final population on the target state  $|n\rangle$  is not perfectly 1 since the blockade subspace has been enlarged.

### C. Nonclassicality

The Fock state is purely nonclassical, in contrast to coherent states which minimize the uncertainty principle and are thus considered classical. However, the quantum behaviors of nanomechanical resonators are easily deteriorated by decoherence. In this section, we explore how our generated state maintains its nonclassical properties in the presence of field damping, as well as parameter mismatching.

We use the Wigner function to identify the state's nonclassicality. Nonnegativity is necessary if we want to interpret the Wigner function as a classical probability distribution. The negative part of the Wigner function is linked with quantum

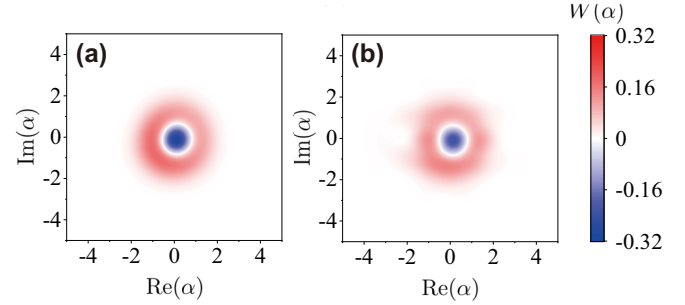


FIG. 7. Wigner function for the generated state (a) without and (b) with dissipation. Parameter mismatches are set to  $\delta r_1 = 0.1$ ,  $\delta r_2 = 0.1$ . The dissipation rate is the same as in Fig. 6 with  $\gamma \approx 0.0033\Lambda$  and  $n_{\text{th}} = 20$ . The Wigner function has strong negativity even in the presence of dissipation, which indicates the state's nonclassical properties.

properties like interference, which makes it a promising indicator that a state is nonclassical [63]. As shown in Fig. 7(b), setting the dissipation rate to be experimentally feasible, the Wigner function of the generated state has only a small deformation compared to the Wigner function of the pure Fock state, and it has strong negative parts. This is not realized in UCPNB where the prepared state's Wigner function is nonnegative [58]. Thus our state's nonclassicality is robust against decoherence.

## IV. DETECTION OF THE FOCK STATE

We need to test how close the prepared state is to the Fock state so that the validity of the preparation method can be verified. We use the average phonon number as an indicator to confirm the excitation level of the oscillator.

We focus on an optomechanical coupling scheme that implements passive optical feedback cooling and can simultaneously measure the average phonon number of the cantilever. The device contains a Michelson interferometer with an optical cavity at the end of each arm (see [64]). A small mirror at the end of one of the optical cavities is mounted on the cantilever. Cavity photons and cantilever phonons are coupled by radiation pressure.

Anti-Stokes and Stokes processes happen at the same time between the cavity and the oscillator, decreasing or increasing the quantum number of the mechanical eigenmode. The optical output spectrum displays two peaks for anti-Stokes and Stokes processes. The phonon number can be measured from the ratio of the peak intensities [65,66].

Integrated optomechanical systems can realize the optical readout of the mechanical mode in various experimental platforms [67,68]. There are many other methods to detect the Fock state, including the use of the nonlinear correlation between the two vibration modes [69], coupling with copper boxes [70], or magnetic resonances [71,72]. The pulsed single-spin measurement can also be applied to measure the motion of its coupled resonator by synchronizing their dynamics [73].

## V. EXPERIMENTAL FEASIBILITY

In the following, we propose a set of parameters that are feasible for experiments. Choose  $(l, w, t) =$

(4, 0.1, 0.01)  $\mu\text{m}$ , modulus  $E \approx 1.22 \times 10^{12}$  Pa, and density  $\rho \approx 3.52 \times 10^3$  kg/m<sup>3</sup> for the resonator. The corresponding mechanical vibration frequency is  $\omega_m \approx 3.516 \times (t/l^2)\sqrt{E/12\rho} \approx 2\pi \times 1.9$  MHz, and the effective mass is  $M = \rho l w t / 4 \approx 3.52 \times 10^{-18}$  kg. Then the zero field fluctuation  $z_{zpf} = \sqrt{\hbar/2M\omega_m} \approx 1.13$  pm. Tune the magnetic field gradient to  $2 \times 10^7$  T/m, the spin-mechanical coupling rate  $g = \frac{1}{2}\mu_B g_e z_{zpf} G \approx 0.314$  MHz.

Tune  $\Omega$  and  $\Delta$  to get  $\omega_{ed} \approx 0.285$  MHz. Now the Duffing nonlinearity  $U = -6.14$  Hz. Set  $\omega_p = 9.84$  MHz. According to Eq. (14c), we have  $\Lambda \approx 3.58$  kHz, and the corresponding displacement  $\alpha = -292$ . Large  $|\alpha|$  is desirable if we want  $\Lambda \gg \gamma$ . The two driving amplitudes are required to be  $\varepsilon_L = 0.610$  GHz and  $\Omega_p = 1.05$  MHz.

Usually, the  $Q$  factor for the nanomechanical resonator is between  $10^5$  and  $10^6$  [23]. Thus the damping constant  $\gamma \approx 11.94$  Hz. The cooling of mechanical oscillators has achieved great progress in different platforms [74–77]. When the environmental temperature is 2 mK, which is reachable in current experimental platforms, the corresponding average thermal phonon number is  $n_{th} \approx 20$ .

## VI. CONCLUSION

We realized the phonon blockade and generated the Fock state in a hybrid spin-mechanical system with weak nonlinearity which can be significantly enhanced by linear drives. We show that, following the time-dependent protocol of modulating phonon drives, there exists a true cutoff in phonon number distribution and an intermediate state at a particular time is an accurate Fock state. The phonon-blockaded physics is robust against imperfections in parameters with the mean phonon number very close to 1 and small second-order correlation functions. The Wigner function of the state has strong negativity even in the presence of dissipation, which indicates its highly nonclassical nature. We also present how to detect our Fock state. The mechanism is valid to generate  $n$ -phonon-blockaded states as well.

## ACKNOWLEDGMENT

This work is supported by the National Natural Science Foundation of China under Grants No. 12375018 and No. 92065105.

- 
- [1] G. Balasubramanian, P. Neumann, D. Twitchen, M. Markham, R. Kolesov, N. Mizuochi, J. Isoya, J. Achard, J. Beck, J. Tjessler, V. Jacques, P. R. Hemmer, F. Jelezko, and J. Wrachtrup, Ultra-long spin coherence time in isotopically engineered diamond, *Nat. Mater.* **8**, 383 (2009).
  - [2] P. Neumann, R. Kolesov, B. Naydenov, J. Beck, F. Rempp, M. Steiner, V. Jacques, G. Balasubramanian, M. L. Markham, D. J. Twitchen, S. Pezzagna, J. Meijer, J. Twamley, F. Jelezko, and J. Wrachtrup, Quantum register based on coupled electron spins in a room-temperature solid, *Nat. Phys.* **6**, 249 (2010).
  - [3] M. W. Doherty, N. B. Manson, P. Delaney, F. Jelezko, J. Wrachtrup, and L. C. Hollenberg, The nitrogen-vacancy colour centre in diamond, *Phys. Rep.* **528**, 1 (2013).
  - [4] H. Wang and I. Lekavicius, Coupling spins to nanomechanical resonators: Toward quantum spin-mechanics, *Appl. Phys. Lett.* **117**, 230501 (2020).
  - [5] M. J. A. Schuetz, E. M. Kessler, G. Giedke, L. M. K. Vandersypen, M. D. Lukin, and J. I. Cirac, Universal quantum transducers based on surface acoustic waves, *Phys. Rev. X* **5**, 031031 (2015).
  - [6] D. A. Golter, T. Oo, M. Amezcua, I. Lekavicius, K. A. Stewart, and H. Wang, Coupling a surface acoustic wave to an electron spin in diamond via a dark state, *Phys. Rev. X* **6**, 041060 (2016).
  - [7] D. A. Golter, T. Oo, M. Amezcua, K. A. Stewart, and H. Wang, Optomechanical quantum control of a nitrogen-vacancy center in diamond, *Phys. Rev. Lett.* **116**, 143602 (2016).
  - [8] P.-B. Li and F. Nori, Hybrid quantum system with nitrogen-vacancy centers in diamond coupled to surface-phonon polaritons in piezomagnetic superlattices, *Phys. Rev. Appl.* **10**, 024011 (2018).
  - [9] B. Li, P.-B. Li, Y. Zhou, J. Liu, H.-R. Li, and F.-L. Li, Interfacing a topological qubit with a spin qubit in a hybrid quantum system, *Phys. Rev. Appl.* **11**, 044026 (2019).
  - [10] O. Arcizet, V. Jacques, A. Siria, P. Poncharal, P. Vincent, and S. Seidelin, A single nitrogen-vacancy defect coupled to a nanomechanical oscillator, *Nat. Phys.* **7**, 879 (2011).
  - [11] S. Kolkowitz, A. C. B. Jayich, Q. P. Unterreithmeier, S. D. Bennett, P. Rabl, J. G. E. Harris, and M. D. Lukin, Coherent sensing of a mechanical resonator with a single-spin qubit, *Science* **335**, 1603 (2012).
  - [12] S. D. Bennett, N. Y. Yao, J. Otterbach, P. Zoller, P. Rabl, and M. D. Lukin, Phonon-induced spin-spin interactions in diamond nanostructures: Application to spin squeezing, *Phys. Rev. Lett.* **110**, 156402 (2013).
  - [13] E. R. MacQuarrie, T. A. Gosavi, N. R. Jungwirth, S. A. Bhawe, and G. D. Fuchs, Mechanical spin control of nitrogen-vacancy centers in diamond, *Phys. Rev. Lett.* **111**, 227602 (2013).
  - [14] I. M. Georgescu, S. Ashhab, and F. Nori, Quantum simulation, *Rev. Mod. Phys.* **86**, 153 (2014).
  - [15] P.-B. Li, Y.-C. Liu, S.-Y. Gao, Z.-L. Xiang, P. Rabl, Y.-F. Xiao, and F.-L. Li, Hybrid quantum device based on NV centers in diamond nanomechanical resonators plus superconducting waveguide cavities, *Phys. Rev. Appl.* **4**, 044003 (2015).
  - [16] P.-B. Li, Z.-L. Xiang, P. Rabl, and F. Nori, Hybrid quantum device with nitrogen-vacancy centers in diamond coupled to carbon nanotubes, *Phys. Rev. Lett.* **117**, 015502 (2016).
  - [17] Y. Ma, Z.-Q. Yin, P. Huang, W. L. Yang, and J. Du, Cooling a mechanical resonator to the quantum regime by heating it, *Phys. Rev. A* **94**, 053836 (2016).
  - [18] C. L. Degen, F. Reinhard, and P. Cappellaro, Quantum sensing, *Rev. Mod. Phys.* **89**, 035002 (2017).
  - [19] M.-A. Lemonde, S. Meesala, A. Sipahigil, M. J. A. Schuetz, M. D. Lukin, M. Loncar, and P. Rabl, Phonon networks with silicon-vacancy centers in diamond waveguides, *Phys. Rev. Lett.* **120**, 213603 (2018).

- [20] C. Sánchez Muñoz, A. Lara, J. Puebla, and F. Nori, Hybrid systems for the generation of nonclassical mechanical states via quadratic interactions, *Phys. Rev. Lett.* **121**, 123604 (2018).
- [21] Y.-F. Qiao, H.-Z. Li, X.-L. Dong, J.-Q. Chen, Y. Zhou, and P.-B. Li, Phononic-waveguide-assisted steady-state entanglement of silicon-vacancy centers, *Phys. Rev. A* **101**, 042313 (2020).
- [22] X.-X. Li, B. Li, and P.-B. Li, Simulation of topological phases with color center arrays in phononic crystals, *Phys. Rev. Res.* **2**, 013121 (2020).
- [23] P.-B. Li, Y. Zhou, W.-B. Gao, and F. Nori, Enhancing spin-phonon and spin-spin interactions using linear resources in a hybrid quantum system, *Phys. Rev. Lett.* **125**, 153602 (2020).
- [24] X.-F. Pan, X.-L. Hei, X.-L. Dong, J.-Q. Chen, C.-P. Shen, H. Ali, and P.-B. Li, Enhanced spin-mechanical interaction with levitated micromagnets, *Phys. Rev. A* **107**, 023722 (2023).
- [25] X.-W. Xu, A.-X. Chen, and Y.-X. Liu, Phonon blockade in a nanomechanical resonator resonantly coupled to a qubit, *Phys. Rev. A* **94**, 063853 (2016).
- [26] X. Wang, A. Miranowicz, H.-R. Li, and F. Nori, Method for observing robust and tunable phonon blockade in a nanomechanical resonator coupled to a charge qubit, *Phys. Rev. A* **93**, 063861 (2016).
- [27] H. Xie, C.-G. Liao, X. Shang, M.-Y. Ye, and X.-M. Lin, Phonon blockade in a quadratically coupled optomechanical system, *Phys. Rev. A* **96**, 013861 (2017).
- [28] H. Xie, C.-G. Liao, X. Shang, Z.-H. Chen, and X.-M. Lin, Optically induced phonon blockade in an optomechanical system with second-order nonlinearity, *Phys. Rev. A* **98**, 023819 (2018).
- [29] L.-L. Zheng, T.-S. Yin, Q. Bin, X.-Y. Lü, and Y. Wu, Single-photon-induced phonon blockade in a hybrid spin-optomechanical system, *Phys. Rev. A* **99**, 013804 (2019).
- [30] T.-S. Yin, Q. Bin, G.-L. Zhu, G.-R. Jin, and A. Chen, Phonon blockade in a hybrid system via the second-order magnetic gradient, *Phys. Rev. A* **100**, 063840 (2019).
- [31] J. Tang, Y. Wu, Z. Wang, H. Sun, L. Tang, H. Zhang, T. Li, Y. Lu, M. Xiao, and K. Xia, Vacuum-induced surface-acoustic-wave phonon blockade, *Phys. Rev. A* **101**, 053802 (2020).
- [32] R. Ohira, S. Kume, K. Takayama, S. Muralidharan, H. Takahashi, and K. Toyoda, Blockade of phonon hopping in trapped ions in the presence of multiple local phonons, *Phys. Rev. A* **103**, 012612 (2021).
- [33] H. Deng, F. Zou, J.-F. Huang, and J.-Q. Liao, Optical normal-mode-induced phonon-sideband splitting in the photon-blockade effect, *Phys. Rev. A* **104**, 033706 (2021).
- [34] W. Xie, Q. Guo, and Z. Duan, Phonon blockade in an acoustic cavity coupled to a three-level artificial atom, *Phys. Rev. B* **106**, 115435 (2022).
- [35] K. M. Birnbaum, A. Boca, R. Miller, A. D. Boozer, T. E. Northup, and H. J. Kimble, Photon blockade in an optical cavity with one trapped atom, *Nature (London)* **436**, 87 (2005).
- [36] A. Faraon, I. Fushman, D. Englund, N. Stoltz, P. Petroff, and J. Vučković, Coherent generation of non-classical light on a chip via photon-induced tunnelling and blockade, *Nat. Phys.* **4**, 859 (2008).
- [37] A. J. Hoffman, S. J. Srinivasan, S. Schmidt, L. Spietz, J. Aumentado, H. E. Türeci, and A. A. Houck, Dispersive photon blockade in a superconducting circuit, *Phys. Rev. Lett.* **107**, 053602 (2011).
- [38] W. Leoński and R. Tanaś, Possibility of producing the one-photon state in a kicked cavity with a nonlinear kerr medium, *Phys. Rev. A* **49**, R20 (1994).
- [39] A. Imamoglu, H. Schmidt, G. Woods, and M. Deutsch, Strongly interacting photons in a nonlinear cavity, *Phys. Rev. Lett.* **79**, 1467 (1997).
- [40] W. Leon-acutecki, Finite-dimensional coherent-state generation and quantum-optical nonlinear oscillator models, *Phys. Rev. A* **55**, 3874 (1997).
- [41] P. Rabl, Photon blockade effect in optomechanical systems, *Phys. Rev. Lett.* **107**, 063601 (2011).
- [42] X.-W. Xu, Y.-J. Li, and Y.-X. Liu, Photon-induced tunneling in optomechanical systems, *Phys. Rev. A* **87**, 025803 (2013).
- [43] D.-Y. Wang, C.-H. Bai, S. Liu, S. Zhang, and H.-F. Wang, Distinguishing photon blockade in a  $\mathcal{PT}$ -symmetric optomechanical system, *Phys. Rev. A* **99**, 043818 (2019).
- [44] A. A. Sokolova, D. A. Kalacheva, G. P. Fedorov, and O. V. Astafiev, Overcoming photon blockade in a circuit-qed single-atom maser with engineered metastability and strong coupling, *Phys. Rev. A* **107**, L031701 (2023).
- [45] A. Lingenfelter, D. Roberts, and A. A. Clerk, Unconditional fock state generation using arbitrarily weak photonic nonlinearities, *Sci. Adv.* **7**, eabj1916 (2021).
- [46] Y.-X. Liu, A. Miranowicz, Y. B. Gao, J. Bajer, C. P. Sun, and F. Nori, Qubit-induced phonon blockade as a signature of quantum behavior in nanomechanical resonators, *Phys. Rev. A* **82**, 032101 (2010).
- [47] J. R. Johansson, N. Lambert, I. Mahboob, H. Yamaguchi, and F. Nori, Entangled-state generation and bell inequality violations in nanomechanical resonators, *Phys. Rev. B* **90**, 174307 (2014).
- [48] X.-Y. Yao, H. Ali, F.-L. Li, and P.-B. Li, Nonreciprocal phonon blockade in a spinning acoustic ring cavity coupled to a two-level system, *Phys. Rev. Appl.* **17**, 054004 (2022).
- [49] N. Didier, S. Pugnetti, Y. M. Blanter, and R. Fazio, Detecting phonon blockade with photons, *Phys. Rev. B* **84**, 054503 (2011).
- [50] A. Miranowicz, J. Bajer, N. Lambert, Y.-X. Liu, and F. Nori, Tunable multiphonon blockade in coupled nanomechanical resonators, *Phys. Rev. A* **93**, 013808 (2016).
- [51] T. Ramos, V. Sudhir, K. Stannigel, P. Zoller, and T. J. Kippenberg, Nonlinear quantum optomechanics via individual intrinsic two-level defects, *Phys. Rev. Lett.* **110**, 193602 (2013).
- [52] H. Seok and E. M. Wright, Antibunching in an optomechanical oscillator, *Phys. Rev. A* **95**, 053844 (2017).
- [53] X.-W. Xu, H.-Q. Shi, A.-X. Chen, and Y.-X. Liu, Cross-correlation between photons and phonons in quadratically coupled optomechanical systems, *Phys. Rev. A* **98**, 013821 (2018).
- [54] K. Cai, Z.-W. Pan, R.-X. Wang, D. Ruan, Z.-Q. Yin, and G.-L. Long, Single phonon source based on a giant polariton nonlinear effect, *Opt. Lett.* **43**, 1163 (2018).
- [55] G.-W. Deng, D. Zhu, X.-H. Wang, C.-L. Zou, J.-T. Wang, H.-O. Li, G. Cao, D. Liu, Y. Li, M. Xiao *et al.*, Strongly coupled nanotube electromechanical resonators, *Nano Lett.* **16**, 5456 (2016).
- [56] S. Guan, W. P. Bowen, C. Liu, and Z. Duan, Phonon antibunching effect in coupled nonlinear micro/nanomechanical resonator at finite temperature, *Europhys. Lett.* **119**, 58001 (2017).

- [57] W. Mei, T.-S. Yin, Z.-Y. Sun, H.-G. Cheng, B.-F. Zhan, and L.-L. Zheng, Unconventional phonon blockade via atom-photon-phonon interaction in hybrid optomechanical systems, *Opt. Express* **30**, 10251 (2022).
- [58] M.-A. Lemonde, N. Didier, and A. A. Clerk, Antibunching and unconventional photon blockade with gaussian squeezed states, *Phys. Rev. A* **90**, 063824 (2014).
- [59] P. Rabl, P. Cappellaro, M. V. G. Dutt, L. Jiang, J. R. Maze, and M. D. Lukin, Strong magnetic coupling between an electronic spin qubit and a mechanical resonator, *Phys. Rev. B* **79**, 041302(R) (2009).
- [60] Y. Wang, J.-L. Wu, J.-X. Han, Y. Xia, Y.-Y. Jiang, and J. Song, Enhanced phonon blockade in a weakly coupled hybrid system via mechanical parametric amplification, *Phys. Rev. Appl.* **17**, 024009 (2022).
- [61] M. Boissonneault, J. M. Gambetta, and A. Blais, Dispersive regime of circuit qed: Photon-dependent qubit dephasing and relaxation rates, *Phys. Rev. A* **79**, 013819 (2009).
- [62] A. Gilchrist, N. K. Langford, and M. A. Nielsen, Distance measures to compare real and ideal quantum processes, *Phys. Rev. A* **71**, 062310 (2005).
- [63] A. Kenfack and K. Życzkowski, Negativity of the Wigner function as an indicator of non-classicality, *J. Opt. B: Quantum Semiclassical Opt.* **6**, 396 (2004).
- [64] D. Kleckner, I. Pikovski, E. Jeffrey, L. Ament, E. Eliel, J. van den Brink, and D. Bouwmeester, Creating and verifying a quantum superposition in a micro-optomechanical system, *New J. Phys.* **10**, 095020 (2008).
- [65] I. Wilson-Rae, N. Nooshi, W. Zwerger, and T. J. Kippenberg, Theory of ground state cooling of a mechanical oscillator using dynamical backaction, *Phys. Rev. Lett.* **99**, 093901 (2007).
- [66] F. Marquardt, J. P. Chen, A. A. Clerk, and S. M. Girvin, Quantum theory of cavity-assisted sideband cooling of mechanical motion, *Phys. Rev. Lett.* **99**, 093902 (2007).
- [67] J. Guo and S. Gröblacher, Integrated optical-readout of a high-q mechanical out-of-plane mode, *Light Sci. Appl.* **11**, 282 (2022).
- [68] Y. Yu, X. Xi, and X. Sun, Observation of mechanical bound states in the continuum in an optomechanical microresonator, *Light Sci. Appl.* **11**, 328 (2022).
- [69] D. H. Santamore, A. C. Doherty, and M. C. Cross, Quantum nondemolition measurement of fock states of mesoscopic mechanical oscillators, *Phys. Rev. B* **70**, 144301 (2004).
- [70] E. K. Irish and K. Schwab, Quantum measurement of a coupled nanomechanical resonator-cooper-pair box system, *Phys. Rev. B* **68**, 155311 (2003).
- [71] C. Gonzalez-Ballester, J. Gieseler, and O. Romero-Isart, Quantum acoustomechanics with a micromagnet, *Phys. Rev. Lett.* **124**, 093602 (2020).
- [72] M. F. Colombano, G. Arregui, F. Bonell, N. E. Capuj, E. Chavez-Angel, A. Pitanti, S. O. Valenzuela, C. M. Sotomayor-Torres, D. Navarro-Urrios, and M. V. Costache, Ferromagnetic resonance assisted optomechanical magnetometer, *Phys. Rev. Lett.* **125**, 147201 (2020).
- [73] S. D. Bennett, S. Kolkowitz, Q. P. Unterreithmeier, P. Rabl, A. C. B. Jayich, J. G. E. Harris, and M. D. Lukin, Measuring mechanical motion with a single spin, *New J. Phys.* **14**, 125004 (2012).
- [74] A. D. O'Connell, M. Hofheinz, M. Ansmann, R. C. Bialczak, M. Lenander, E. Lucero, M. Neeley, D. Sank, H. Wang, M. Weides, J. Wenner, J. M. Martinis, and A. N. Cleland, Quantum ground state and single-phonon control of a mechanical resonator, *Nature (London)* **464**, 697 (2010).
- [75] J. D. Teufel, T. Donner, D. Li, J. W. Harlow, M. S. Allman, K. Cicak, A. J. Sirois, J. D. Whittaker, K. W. Lehnert, and R. W. Simmonds, Sideband cooling of micromechanical motion to the quantum ground state, *Nature (London)* **475**, 359 (2011).
- [76] J. Chan, T. P. M. Alegre, A. H. Safavi-Naeini, J. T. Hill, A. Krause, S. Gröblacher, M. Aspelmeyer, and O. Painter, Laser cooling of a nanomechanical oscillator into its quantum ground state, *Nature (London)* **478**, 89 (2011).
- [77] J. B. Clark, F. Lecocq, R. W. Simmonds, J. Aumentado, and J. D. Teufel, Sideband cooling beyond the quantum backaction limit with squeezed light, *Nature (London)* **541**, 191 (2017).